BIOCHEMISTRY
including biophysical chemistry & molecular biology
Article

Biochemistry **2009,** *48,* 4699–4706 4699
DOI: 10.1021/bi900222e

Interaction of IF2 with the Ribosomal GTPase-Associated Center during 70S Initiation Complex Formation†

Haiou Qin, Christina Grigoriadou,‡ and Barry S. Cooperman*

Department of Chemistry, University of Pennsylvania, Philadelphia, Pennsylvania 19104-6323‡ Current address: Department of Molecular Oncology, Genentech Inc., 1 DNA Way, South San Francisco, CA 94080-4918

Received February 10, 2009; Revised Manuscript Received March 27, 2009

ABSTRACT: Addition of an *Escherichia coli* 50S subunit ($50S^{Cy5}$) containing a Cy5-labeled L11 N-terminal domain (L11-NTD) within the GTPase-associated center (GAC) to an *E. coli* 30S initiation complex ($30SIC^{Cy3}$) containing Cy3-labeled initiation factor 2 complexed with GTP leads to rapid development of a FRET signal during formation of the 70S initiation complex (70SIC). Initiation factor 2 (IF2) and elongation factor G (EF-G) induce similar changes in ribosome structure. Here we show that such similarities are maintained on a dynamic level as well. Thus, movement of IF2 toward L11-NTD after initial 70S ribosome formation follows GTP hydrolysis and precedes P_i release, paralleling movement of EF-G following its binding to the ribosome [Seo, H., et al. (2006) *Biochemistry 45*, 2504−2514], and in both cases, the rate of such movement is slowed if GTP hydrolysis is prevented. The $30SIC^{Cy3}$:$50S^{Cy5}$ FRET signal also provides a sensitive probe of the ability of initiation factor 3 to discriminate between a canonical and a noncanonical initiation codon during 70SIC formation. We employ *Bacillus stearothermophilus* IF2 as a substitute for *E. coli* IF2 to take advantage of the higher stability of the complexes it forms with *E. coli* ribosomes. While Bst-IF2 is fully functional in formation of *E. coli* 70SIC, relative reactivities toward dipeptide formation of 70SICs formed with the two IF2s suggest that the Bst-IF2·GDP complex is more difficult to displace from the GAC than the *E. coli* IF2·GDP complex.

Initiation factor 2 (IF2) is a G-protein that plays a crucial role in the initiation of prokaryotic protein synthesis, interacting directly with $fMet\text{-}tRNA^{fMet}$, favoring its decoding in the P-site, and physically linking the 30S and 50S subunits in the 70S initiation complex (70SIC)[1] (*1*−*5*). It shares a common binding locus on the ribosome, the GTPase-associated center (denoted GAC), with other G-proteins utilized in protein synthesis, such as elongation factor G (EF-G). The GAC includes 23 S rRNA helices 42−44, the associated proteins L11 and L10, and at least one L7/L12 protein (*6*, *7*). Cryoelectron microscopy (cryo-EM) studies have indicated that both EF-G·GTP and IF2·GTP binding to the ribosome are accompanied by large conformational changes in the ribosome and that, in both cases, further conformational changes in the ribosome·G-protein complex are seen following GTP hydrolysis (*8*−*12*).

The N-terminal domain of L11 (L11-NTD) is a particularly mobile portion of the ribosome that, following GTP hydrolysis, approaches the G′ domain of EF-G (*9*, *13*, *14*). In earlier work utilizing single-turnover fluorescence resonance energy transfer (FRET) measurements, we determined that rapid movement of the G′ domain toward L11-NTD within the *Escherichia coli* ribosome requires prior GTP hydrolysis and, via branching pathways, either precedes P_i release (major pathway) or occurs simultaneously with it (minor pathway) (*15*). In this latter work, fluorescent groups were placed on Cys 38 within L11-NTD and on a suitable residue within the G′ domain.

Here we utilize a similar approach to determine whether there is a comparable movement toward L11-NTD of the G1 domain of IF2 (IF2 lacks a G′ domain) during 70SIC formation from the 30S initiation complex (30SIC) and 50S subunit. The cryo-EM structures of 70S complexes containing $fMet\text{-}tRNA^{fMet}$, mRNA, and either IF2·GDPCP (a nonhydrolyzable analogue of GTP) or IF2·GDP (*11*) result in an estimated distance of 50−55 Å between the α-carbons of residue 378 in IF2 and residue 38 in L11 (Figure 1), quite suitable for probing by measurement of FRET efficiency. Accordingly, we employ 50S subunits

†This work was supported by NIH Grant GM071014.

*To whom correspondence should be addressed. E-mail: cooprman@pobox.upenn.edu. Telephone: (215) 898-6330. Fax: (215) 898-2037.

[1]Abbreviations: Bst-IF2, G378C-IF2 from *Bacillus stearothermophilus*; $Bst\text{-}IF2^{Cy3}$, Bst-IF2 labeled with Cy3 at position 378; cryo-EM, cryoelectron microscopy; Eco-IF2, IF2 from *Escherichia coli*; FRET, fluorescence resonance energy transfer; GAC, GTPase-associated center; GDPCP and GDPNP, GTP analogues in which the oxygen connecting the β- and γ-phosphorus atoms is replaced with CH_2 and NH groups, respectively; L11-NTD, L11 N-terminal domain; $L11^{Cy5}$, L11 labeled at position 38 with Cy5; MDCC, 7-(diethylamino)-3-({[(2-maleimidyl)ethyl]amino}carbonyl)coumarin; PBP, phosphate binding protein; RFE, relative FRET efficiency; TC, $Phe\text{-}tRNA^{Phe}$·EF-Tu·GTP ternary complex; 30SIC, 30S initiation complex; $30SIC^{Bst}$, $30SIC^{Cy3}$, and $30SIC^{Eco}$, 30SICs made with Bst-IF2, $Bst\text{-}IF2^{Cy3}$, and Eco-IF2, respectively; $50S^{-L11}$, $50S^{L11}$, and $50S^{Cy5}$, 50S subunits isolated from AM77 cells used directly and reconstituted with L11 and $L11^{Cy5}$, respectively; 70SIC, 70S initiation complex.

 Published on Web 04/14/2009

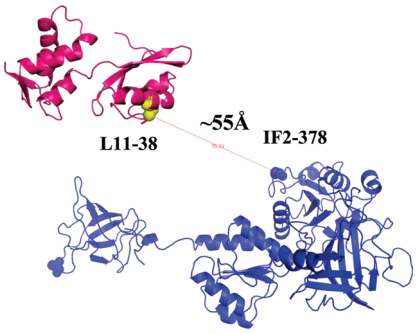

FIGURE 1: Distance between L11 residue 38 and IF2 residue 378 in a 70S·IF2·GMPPCP fMet-tRNA^{fMet}·mRNA complex. According to a cryoelectron microscopy structure [EMD-1172 (*11*)].

containing protein L11 labeled with Cy5 at position 38 (denoted L11^{Cy5}) and *Bacillus stearothermophilus* IF2 (Bst-IF2) labeled with Cy3 at position 378 (denoted Bst-IF2^{Cy3}) (*16*).

Substituting Bst-IF2 for Eco-IF2 has been shown to facilitate the characterization of translation intermediates, due to the higher stability of the complexes that Bst-IF2 forms with *E. coli* ribosomes and ribosomal subunits as compared with Eco-IF2 (*16*, *17*). Such substitution is reasonable in view of substantial evidence that Bst-IF2 is functionally interchangeable with Eco-IF2 in *E. coli* protein synthesis. Thus, Bst-IF2 complements an *E. coli infB* null mutation in vivo (E. Caserta and C. Gualerzi, private communication). In addition, in vitro studies demonstrate the near equivalence of Eco-IF2, Bst-IF2, and Bst-IF2^{Cy3} in binary complex formation with *E. coli* fMet-tRNA^{fMet} (*18*), in stimulation of AUG-dependent fMet-tRNA^{fMet} binding to *E. coli* 30S subunits and 70S ribosomes (*19*) and in kinetic measures of 70SIC formation (refs *17* and *20* and work reported herein).

We find that FRET efficiency increases as the 70S ribosomes formed initially from 30SIC and 50S subunits are transformed into the 70SIC, and that the rate of such an increase depends on GTP hydrolysis, paralleling results obtained with EF-G. We further demonstrate that the increase in FRET efficiency can be used to monitor the fidelity function of initiation factor IF3 during 70SIC formation.

MATERIALS AND METHODS

Proteins. *E. coli* IF1, IF2, and IF3 (*17*, *21*, *22*) and EF-Tu (*23*) were prepared as described previously. The *B. stearothermophilus* G378C-IF2 mutant (Bst-IF2) was prepared as described previously (*20*, *22*). Bst-IF2^{Cy3} was prepared by reacting Bst-IF2 with Cy3-maleimide (GE Healthcare) as described previously (*20*), except that, in addition to incubation at room temperature for 2 h, the reaction mixture was also kept overnight at 4 °C. Under these conditions, IF2 was labeled quantitatively with Cy3, as calculated using an ε_{550} (Cy3) equal to 150000 M^{-1} cm^{-1} (*24*) and estimating the Bst-IF2 concentration by the Bradford assay (*25*). MDCC-labeled phosphate-binding protein (PBP) (*15*) and N-terminally His-tagged L11 were prepared essentially as described previously (*26*). L11^{Cy5} was prepared by reacting L11 at its unique Cys (position 38) with Cy5-maleimide (GE Healthcare) following the method of Wang et al. (*26*).

tRNA and mRNA. ^{35}S-labeled fMet-tRNA^{fMet}, fMet-tRNA^{fMet}(prf20), Phe-tRNA^{Phe}, and 022AUG and 022AUU mRNAs were prepared as described previously (*23*, *27*−*29*).

Ribosomes and Subunits. Tight couple wild-type 70S ribosomes and 30S and 50S subunits were isolated from MRE600 as described previously (*20*). Mutant 70S ribosomes lacking L11 were isolated from *E. coli* strain AM77 as described previously (*15*) except that zonal gradient purification was conducted in a buffer containing 8 mM Mg^{2+} rather than 6 mM Mg^{2+}. AM77 50S subunits, denoted 50S^{-L11}, were prepared from AM77 70S ribosomes as described for wt-50S subunits (*20*).

Reconstituted 50S Subunits. 50S subunits containing Cy5-labeled L11 (denoted 50S^{Cy5}) were prepared by incubating L11^{Cy5} (1 nmol, measured as Cy5) with 1 nmol of 50S^{-L11} subunits in buffer A [25 mM Tris (pH 7.6), 30 mM NH_4Cl, 70 mM KCl, 7 mM $MgCl_2$, and 1 mM dithiothreitol] for 15 min at 37 °C. Unbound L11^{Cy5} and any residual unincorporated dye were removed by ultracentrifugation for 18 h through a 1.1 M sucrose cushion in buffer A in rotor type 70.1Ti at 220000*g*, yielding 50S^{Cy5} which contained 1.0 ± 0.2 Cy5/subunit. A control reconstitution experiment performed with wild-type MRE 600 50S subunits resulted in a Cy5:50S subunit ratio of < 0.2. 50S subunits reconstituted from 50S^{-L11} subunits and unlabeled L11 (denoted 50S^{L11}) were prepared similarly.

Complexes. Preformed complexes were incubated for 15 min at 37 °C prior to being used. 30SIC was always formed by incubation of 1.0 equiv of 30S subunits with 1.5 equiv of IF1, IF3, and fMet-tRNA^{fMet}, 3.0 equiv of mRNA, and various amounts of IF2. 30SICs made up with Eco-IF2, Bst-IF2, and Bst-IF2^{Cy3} are denoted 30SIC^{Eco}, 30SIC^{Bst}, and 30SIC^{Cy3}, respectively. Ternary complex (TC) was formed by incubation of 1.0 equiv of [^{3}H]Phe-tRNA^{Phe} with 1.5 equiv of EF-Tu and 200 μM GTP. The TC concentration is calculated as the concentration of [^{3}H]Phe-tRNA^{Phe}. 70SIC was preformed by incubation of 30SIC (0.3 μM) with 50S subunits (0.5 μM) in buffer A.

Equilibrium and Kinetic Measurements. All concentrations specified in the text and figure legends refer to final concentrations after mixing unless otherwise specified. All equilibrium and kinetic experiments involving fluorescence measurements, GTP hydrolysis, and peptide bond formation were performed in buffer A at 20 °C.

Equilibrium Fluorescence. Solutions were excited at 540 nm, and emission was monitored from 560 to 720 nm (SPEX Fluorolog-3, Jobin Yvon Inc.).

Light Scattering, IF2^{Cy3} Fluorescence, 50S^{Cy5} Fluorescence, and P_i Release. Measurements were performed in either an SX.18MV (Applied Photophysics) or a KinTec SF-2004 stopped-flow spectrophotometer by rapid mixing of 30S complexes with 50S subunits. Light scattering and P_i release were measured as described previously (*20*). For IF2^{Cy3} and 50S^{Cy5} fluorescence, excitation was at 540 nm and output was monitored at 567 nm and either at 670 nm or using a 680 ± 10 nm bandpass filter (Figure 7), respectively.

GTPase Activity, fMet-Puromycin Formation, and fMetPhe-tRNA^{Phe} Formation. Measurements were performed in a KinTec RQF-3 apparatus. Rates of GTPase were determined by rapid mixing of 30 complexes with 50S subunits followed by rapid quenching, as described previously (*20*). Rates of [^{35}S]fMet-puromycin formation were determined by rapid mixing of preformed 70SIC with the puromycin, followed by quenching with 0.3 M sodium acetate (pH 5.2), extraction with ethyl acetate, and determination of the radioactivity in the ethyl acetate layer. Rates of fMetPhe-tRNA^{Phe} formation were determined as described previously (*20*), by rapid mixing of either 30S complexes with 50S subunits and the Phe-tRNA^{Phe}·EF-Tu·GTP ternary complex or preformed 70SIC with the ternary complex, followed by rapid quenching.

Kinetic Analyses. Apparent rate constants and microscopic constants for specific kinetic schemes were determined using Igor-Pro [Wavemetrics, for single-, double-, and triple-exponential equations (Tables 1 and 2 and Figure 6)] and Scientist [MicroMath Research, LC, for global fitting of multiple parameters to Scheme 1 (Figure 5C)].

Poly(U)-Dependent Poly(Phe) Synthesis. The assay was conducted as described previously (*26*), except that 70S ribosomes were formed by preincubation of 50S subunits (0.5 μM) with 30S subunits (1.0 μM) for 15 min at 37 °C.

R_o and FRET Efficiency Estimation. The Förster distance (R_o) was calculated from eq 1, where ϕ_D is the quantum yield of 30SIC^{Cy3}, η is the refractive index of water [1.33 (*30*)], κ^2 is a dipole orientation factor and was set equal to $^2/_3$ assuming random orientations of the fluorophores (*31*, *32*), and $J(\lambda)$ is the spectral overlap integral. ϕ_D was determined by comparing the integrated fluorescence of 30SIC^{Cy3} to that of a standard, Rhodamine B, as described previously (*31*), yielding a value of 0.57 ± 0.03. $J(\lambda)$, equal to 4.66×10^{-13} M^{-1} cm^3, was determined from the fluorescence and absorption spectra of 30SIC^{Cy3} and 50S^{Cy5}, respectively. These values permit calculation of an R_o equal to 60 ± 5 Å, in good agreement with other reported values of 50−60 Å for the Cy3/Cy5 pair (*33*, *34*).

$$R_o\,(\text{é}) = [8.8 \times 10^{-5} \times \kappa^2 \eta^{-4} \phi_D J(\lambda)]^{1/6} \quad (1)$$

FRET efficiency, E, was calculated from eq 2, where F_{DA} and F_A are the background-corrected fluorescence values of the donor/acceptor pair and the acceptor alone, respectively, on irradiation at the excitation wavelength (λ_{ex}) of the donor (540 nm) and detection at the emission maximum of the acceptor, λ_A (670 nm), f_D is a fractional labeling of donor (equal to 1.0), and ε_A and ε_D are the extinction coefficients of the donor and acceptor at λ_{ex}, respectively.

$$E = \left[\frac{\varepsilon_A(\lambda_{ex})}{\varepsilon_D(\lambda_{ex})}\right]\left[\frac{F_{DA}(\lambda_A)}{F_A(\lambda_A)} - 1\right]\left(\frac{1}{f_D}\right) \quad (2)$$

RESULTS

In the work described below, we use the FRET signal between a 30SIC containing Bst-IF2^{Cy3} and a 50S subunit containing L11^{Cy5} to monitor the relative movement of IF2 with respect to L11 during 70SIC formation. Below, we first demonstrate that, with minor qualifications, Bst-IF2^{Cy3} and L11^{Cy5} are acceptable functional analogues of Eco-IF2 and unlabeled L11, respectively, before presenting our FRET results.

Bst-IF2 and Bst-IF2^{Cy3} as Functional Analogues of Eco-IF2 with Respect to 70SIC Formation and Reactivity. In the presence of IF3, association of 30S with 50S subunits to form 70SIC is completely dependent on the presence of IF2 (*20*). Here we carry out four rapid kinetics measures [increase in light scattering, IF2-dependent single-turnover GTP hydrolysis, and subsequent P_i release, and increase in fMet-tRNA^{fMet}(prf20) fluorescence] that we previously employed in formulating a detailed quantitative kinetic scheme for formation of 70SIC from 30SIC and the 50S subunit (*20*) to compare the functionalities of Eco-IF2 (30SIC^{Eco}), BSt-IF2 (30SIC^{Bst}), and Bst-IF2^{Cy3} (30SIC^{Cy3}) in this process. We also compare the reactivities of the three 70SICs formed during dipeptide formation. Our results show that all three 30SICs have similar rates of 70SIC formation, but that the reactivity of the 70SIC in dipeptide formation is somewhat faster in the presence of Eco-IF2 versus either of the Bst-IF2s.

Table 1: Functionality of Different 30SICs with Respect to 70SIC Formation and Reactivity[a]

apparent rate constant (s^{-1})	30SIC^{Eco}	30SIC^{Bst}	30SIC^{Cy3}
LS1	61 ± 5	82 ± 5	65 ± 3
LS2	10 ± 1	8 ± 1	10 ± 1
GTP1	64 ± 13	53 ± 8	40 ± 2
fMet1	4.1 ± 0.4	5.2 ± 0.5	–
fMet2	1.6 ± 0.3	2.1 ± 0.2	–
P_i1	7.0 ± 0.5	7.0 ± 0.5	7.0 ± 0.5
P_i2	1.5 ± 0.1	1.3 ± 0.1	1.4 ± 0.1
k'_{dp}[b]	0.28 ± 0.06	0.14 ± 0.03	0.18 ± 0.06
k^*_{dp}[c]	1.6 ± 0.2	0.12 ± 0.02	–

[a] Reaction conditions as described in the legend of Figure 2. [b] Dipeptide formation, rapid mixing of 30SIC with 50S subunits and cognate TC. [c] Dipeptide formation, rapid mixing of 70SIC with cognate TC.

Table 2: Apparent Rate Constants and Reaction Stoichiometries for 50S Subunit Function in 70SIC Formation

parameter	wt-50S	50S^{-L11}	50S^{L11}	50S^{Cy5}
GTP1 (s^{-1})	41 ± 3	23 ± 6	37 ± 9	29 ± 6
P_i/IF2	0.85 ± 0.05	0.48 ± 0.04	0.83 ± 0.07	0.83 ± 0.04
k'_{dp} (s^{-1})	0.18 ± 0.06	–	–	0.07 ± 0.01
fMetPhe/IF2	0.65 ± 0.07	–	–	0.66 ± 0.04
k'_{puro} (s^{-1})	0.42 ± 0.05	–	–	0.33 ± 0.04
fMet-puro/IF2	0.75 ± 0.03	–	–	0.65 ± 0.03

The increase in light scattering upon addition of 30SIC to the 50S subunit is well-described as a two-phase process (Figure 2A), with the first corresponding to initial binding of the 50S subunit to 30SIC to form a labile 70S complex and the second reflecting conversion to the more stable 70SIC. These two phases have apparent rate constants LS1 and LS2. Initial 70S formation is followed by GTP hydrolysis (Figure 2B), with an apparent rate constant (GTP1) that is similar to or somewhat smaller than LS1. P_i release proceeds via a lag phase, with an apparent rate constant P_i1, similar in magnitude to LS2, followed by the P_i release step, with an apparent rate constant P_i2 (Figure 2C). The increase in fluorescence of fMet-tRNA^{fMet}(prf20) on 70SIC formation, which could not be measured for Bst-IF2^{Cy3} because of fluorophore interference, is also preceded by a lag phase (Figure 2D), with apparent rate constants for both phases, fMet1 and fMet2, that are similar in magnitude to the values of P_i1 and P_i2.

Values for each of the apparent rate constants mentioned above are listed in Table 1. From these values, as well as by direct inspection of Figure 2A−D, we conclude that 70SIC formation proceeds in a very similar manner with either 30SIC^{Eco}, 30SIC^{Bst}, or 30SIC^{Cy3}. Some small quantitative differences include larger overall light scattering changes falling in the order Bst-IF2^{Cy3} > Bst-IF2 > Eco-IF2 and GTP1 values decreasing in the order Eco-IF2 > BSt-IF2 > Bst-IF2^{Cy3}.

The functionality of the three 70SIC complexes in fMetPhe-tRNA^{Phe} formation on addition of the Phe-tRNA^{Phe}·EF-Tu·GTP ternary complex was determined either following rapid mixing of each of the preformed 30SICs with 50S subunits and the cognate TC or following rapid mixing of each of the preformed 70SICs with cognate TC (Figure 2E and Table 2). Comparable reactivities (k'_{dp}) were found following the first protocol, with apparent rate constants falling in the order

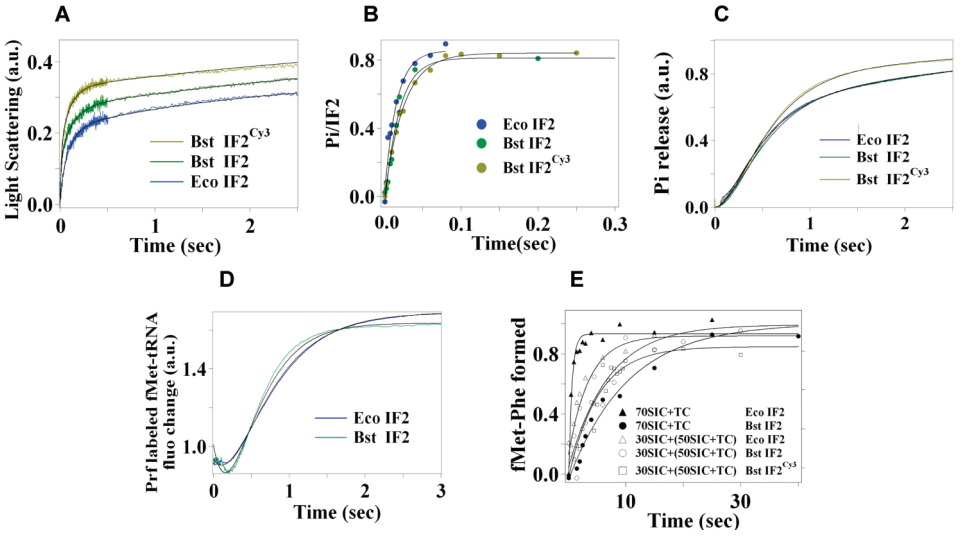

FIGURE 2: Measures of 70SIC formation and reactivity using different 30SICs: (A) light scattering, (B) GTP hydrolysis, (C) P_i release, (D) fMet-tRNA^{fMet}(prf) fluorescence, and (E) fMetPhe-tRNA^{Phe} formation. Experiments in panels A, C, and D were conducted by rapid mixing of the various 30SICs with wt-50S subunits in a stopped-flow spectrofluorometer. In all experiments except those depicted in panel E with preformed 70SIC, 30S and 50S subunits were present at final concentrations of 0.3 and 0.5 μM, respectively. Preformed 70SIC in panel E was present at a concentration of 0.3 μM. Other final concentrations were 0.15 μM IF2 (A and E) and 0.45 μM IF2 (B–D); 100 μM GTP (A, C, and D), 36 μM GTP (B), and 200 μM GTP (E); and 1.0 μM TC (E).

30SIC^{Eco} (0.28 ± 0.06 s^{-1}) > 30SIC^{Cy3} (0.18 ± 0.06 s^{-1}) ~ 30SIC^{Bst} (0.14 ± 0.03 s^{-1}). On the other hand, the second protocol, while leaving the apparent rate constant (k^*_{dp}) for 30SIC^{Bst} essentially unchanged (0.12 ± 0.02 s^{-1}), leads to a marked increase in k^*_{dp} found with 30SIC^{Eco} (1.6 ± 0.2 s^{-1}).

The latter difference may be related to the more stable binding within the 70SIC of Bst-IF2·GDP than Eco-IF2·GDP (*17*, *35*). Thus, productive binding of TC leading to dipeptide formation requires, at a minimum, movement of IF2 away from its canonical position within the 70SIC (*11*), allowing TC binding to the GAC, if not full dissociation of IF2 from the ribosome. Such movement (or dissociation) might be partially rate-determining for dipeptide formation when the 50S subunit and TC are added simultaneously to 30SIC, consistent with earlier results of Tomsic et al. (*36*), but might already be completed, at least for the more weakly bound Eco-IF2, when TC is added to preformed 70SIC, resulting in more rapid dipeptide formation.

50S^{Cy5} as a Functional Analogue of wt-50S with Respect to 70SIC Formation and Reactivity. Having established the functionality of 30SIC^{Cy3}, we next use 30S^{Cy3} to compare 50S^{Cy5} with wt-50S with respect to three single-turnover kinetic (GTP1 and the apparent rate constants for dipeptide and fMet-puromycin formation) and three single-turnover stoichiometric (GTPase, dipeptide, and fMet-puromycin) measures of 70SIC formation and reactivity. The results, as displayed in Figure 3A,B and Table 2 (along with more limited results for 50S^{L11} and 50S^{-L11}), show 50S^{Cy5} to be a good functional analogue of wt-50S, with the only significant difference in these six measures being found for the value of k'_{dp} (fMet-Phe formation), 0.18 ± 0.06 and 0.07 ± 0.01 s^{-1} for wt-50S and 50S^{Cy5}, respectively. Furthermore, preformed 70S ribosomes have virtually identical activities in poly(U)-dependent poly(Phe) synthesis, whether they are made with wt-50S or 50S^{Cy5} subunits (Figure 3C).

There is a significant decrease in the GTPase stoichiometry obtained with 50S^{-L11} subunits (Figure 3A and Table 2), consistent with earlier results showing that 50S^{-L11} subunits are somewhat defective in forming 70SIC from 30SIC (*37*, *38*). However, even the 50S^{-L11} subunits exhibit appreciable activity

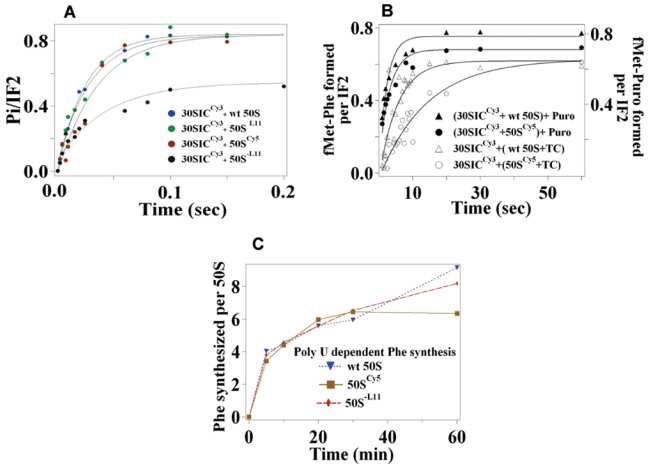

FIGURE 3: Measures of 70SIC formation and reactivity using different 50S subunits: (A) GTP hydrolysis, (B) fMetPhe-tRNA^{Phe} and fMet-puromycin formation, and (C) poly(U)-dependent poly(Phe) synthesis. fMetPhe-tRNA^{Phe} formation was conducted by rapid mixing of 30SIC^{Cy3} with 50S subunits and the Phe-tRNA^{Phe}·EF-Tu·GTP ternary complex. Final concentrations were 0.5 μM 50S, 0.3 μM 30S, and 0.15 μM IF2. Other final concentrations were 36 μM GTP (A), 200 μM GTP (B), and 2.5 mM puromycin (B). (C) See Materials and Methods. Results with wt-50S and 50S^{-L11} parallel those reported previously (*40*).

in poly(Phe) synthesis (Figure 3C), in agreement with previous results (*39*, *40*).

FRET Changes Accompanying Formation of 70SIC from 30SIC^{Cy3} and 50S^{Cy5}. The experiments described above establish the basic functionality of 30SIC^{Cy3} and 50S^{Cy5} in 70SIC formation, making it likely that the FRET experiments described below that measure FRET during the combination of these modified subunits will be relevant for understanding the process of formation of 70SIC from native, unmodified subunits. Long-term incubation (15 min at 37 °C) of 30SIC^{Cy3}, containing a fluorescent donor (D), with 50S^{Cy5} subunits containing a fluorescence acceptor (A) results in formation of the double-labeled 70SIC (DA sample) and the generation of a strong FRET signal

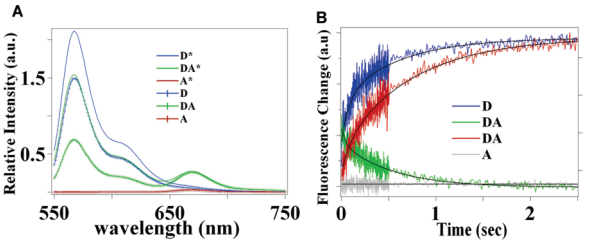

FIGURE 4: FRET between $L11^{Cy5}$ and Bst-$IF2^{Cy3}$ in the 70SIC complex (A) after 70SIC formation and (B) during 70SIC formation. Excitation was at 540 nm. DA samples contained $30SIC^{Cy3}$ and $50S^{Cy5}$. D samples contained $30SIC^{Cy3}$ and $50S^{L11}$. A samples contained $30SIC^{Bst}$ and $50S^{Cy5}$. In panel A, 30SIC and 50S subunits were incubated at 37 °C for 15 min before fluorescence spectra were recorded. Final concentrations were 0.3 μM 30S (hatched lines) or 0.6 μM 30S (smooth lines); 0.15 μM Bst-IF2 or Bst-$IF2^{Cy3}$ (hatched lines) or 0.3 μM Bst-IF2 or Bst-$IF2^{Cy3}$ (smooth lines); 0.14 μM $50S^{L11}$ or $50S^{Cy5}$; and 100 μM GTP. In panel B, 30SICs were rapidly mixed with 50S subunits. The D and A samples were monitored at 567 and 670 nm, respectively. The DA samples were monitored at both wavelengths, as indicated. Final concentrations were 0.30 μM 30S, 0.25 μM IF2, 0.18 μM 50S, and 100 μM GTP.

(Figure 4A), with considerable decreases and increases in donor and acceptor fluorescence signals, respectively, as compared with the fluorescence of the D ($30SIC^{Cy3}$ with $50S^{L11}$) and A ($30SIC^{Bst}$ with $50S^{Cy5}$) samples. In fact, the donor decrease shown in Figure 4A underestimates FRET efficiency, given the intrinsic increase in donor fluorescence that accompanies 70SIC formation when $30SIC^{Cy3}$ is rapidly mixed with unlabeled $50S^{L11}$ subunits (Figure 4B). By contrast, there is no corresponding change in acceptor fluorescence when $30SIC^{Bst}$ replaces $30SIC^{Cy3}$ (Figure 4B). The similarity in acceptor fluorescence intensity at the two $30SIC^{Cy3}$ concentrations employed in Figure 4A indicates that essentially all of $50S^{Cy5}$ is taken up within the 70SIC at the higher 30SIC concentration. These results permit calculation of a FRET efficiency in the 70SIC complex of ~50% by application of eq 2 (Materials and Methods).

Changes in FRET versus Changes in Light Scattering during 70SIC Formation. Strong evidence that the FRET signals seen in Figure 4 are a direct consequence of 70SIC formation is provided by results in Figure 5A showing no such appearance of a FRET signal, measured as the increase in Cy5 fluorescence, when fMet-$tRNA^{fMet}$ is omitted from the reaction mixture. This is in accord with results showing that, in the presence of IF3, fMet-$tRNA^{fMet}$ is required for 70SIC formation (*20*, *41*, *42*).

The increase in light scattering on formation of 70SIC from 30SIC and the 50S subunit provides another measure of 70SIC formation (*20*). Comparison of the time dependence of the increase in FRET efficiency for the complete system (i.e., including fMet-$tRNA^{fMet}$) with the corresponding increase in light scattering, measured on identical samples (Figure 5A), clearly shows that both increases proceed in more than one phase, with both showing an initial rapid phase that is somewhat more pronounced for the light scattering change (*20*) than for the FRET change. As with FRET change, the rapid increase in light scattering is abolished when fMet-$tRNA^{fMet}$ is omitted.

The experiments shown in Figure 5A were conducted with both $IF2^{Cy3}$ and $50S^{Cy5}$ subunits present in excess over 30S subunits. Under these conditions, the time courses of FRET and light scattering increases are directly comparable, with virtually all 30S subunits in the sample containing $IF2^{Cy3}$ as part of 30SIC and all $30SIC^{Cy3}$ interacting with $50S^{Cy5}$. Other conditions, such

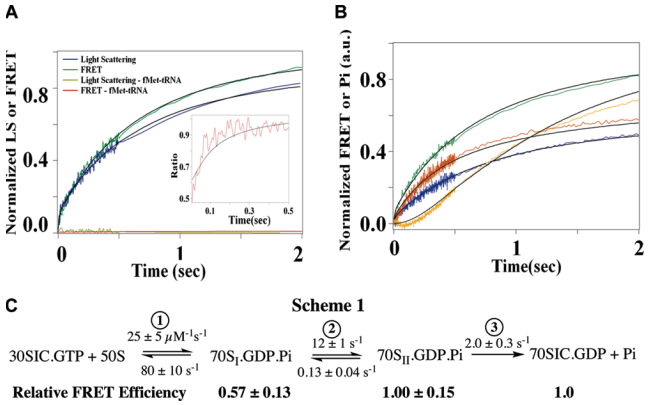

FIGURE 5: Measures of 70SIC formation upon combination of $30SIC^{Cy3}$ and $50S^{Cy5}$: FRET, light scattering, and P_i formation. (A) Direct comparison of FRET (green trace, acceptor fluorescence, excitation at 540 nm, monitoring at 670 nm) and light scattering (blue trace, irradiation at 436 nm, monitoring via a 455 nm cutoff filter) changes during 70SIC formation. Both traces were determined for an identical solution having the following final concentrations: 0.3 μM 30S, 0.45 μM Bst-$IF2^{Cy3}$, and 0.60 μM $50S^{Cy5}$. For ease of comparison, the changes in each value were normalized to the total change seen at the plateau for each measurement (~10 s). The ratio of normalized FRET change to normalized light scattering change is plotted in the inset. When fMet-$tRNA^{fMet}$ was omitted, virtually no changes were seen in either FRET (red trace) or light scattering (yellow trace). (B) FRET changes (green, red, and blue traces) and P_i formation (orange trace). Final concentrations employed: 0.3 μM 30S, 0.45 μM Bst-$IF2^{Cy3}$, and 0.60 μM $50S^{Cy5}$ for green and orange traces; 0.6 μM 30S, 0.50 μM Bst-$IF2^{Cy3}$, and 0.18 μM $50S^{Cy5}$ for the blue trace; and 0.3 μM 30S, 0.25 μM Bst-$IF2^{Cy3}$, and 0.50 μM $50S^{Cy5}$ for the red trace. FRET changes are normalized for the total change seen at the plateau for the green trace, as in panel A. The P_i release is normalized for the total change seen at the plateau, achieved at ~5 s. The final GTP concentration in panels A and B was 100 μM. All solid black lines are fits of the data to Scheme 1, with an R^2 of 0.997 (R^2 is the square of the sample correlation coefficient between the outcomes and their predicted values). Attempts to fit the results in panels A and B to a two-step model resulted in significantly lower R^2 values. (C) Scheme 1, the minimal scheme accounting quantitatively for 70SIC formation in the presence of GTP.

as those employed in Figure 5B (30S > $IF2^{Cy3}$ > $50S^{L11}$; 50S > 30S > $IF2^{Cy3}$), lead to multiphasic increases in light scattering that reflect sample heterogeneity and are unsuitable for directly comparing increases in FRET and light scattering. Thus, slow phases of light scattering are observed when either the 50S subunit concentration is limiting, due to the presence of a minor fraction (<20%) of 50S subunits that lack L11 ($50S^{-L11}$) and form 70SIC complexes only very slowly (data not shown; see also refs *37* and *38*), or $IF2^{Cy3}$ is limiting, since 30S initiation complexes formed in the presence of IF3 but lacking IF2 also form 70SIC very slowly (*20*). Such sample heterogeneity is not a problem for FRET measurements, which measure only rapid 70SIC formation events between 30SICs containing Bst-$IF2^{Cy3}$ and 50S subunits containing $L11^{Cy5}$. The rate of P_i release is also shown in Figure 5B for direct comparison with the rate of FRET increase.

The results in panels A and B of Figure 5 provide clear evidence that 70SIC formation, culminating with P_i release, proceeds in a minimum of three phases. Thus, the change in the ratio of normalized FRET change to normalized light scattering change, which is completed within 0.1 s (Figure 5A, inset), demonstrates an initial rapid phase, while the slower overall increase in the magnitude of the FRET signal, indicative of phase 2, clearly proceeds more rapidly than P_i release

(Figure 5B), which proceeds in phase 3. These results can be globally fit to the minimal Scheme 1 (Figure 5C), in which an initial binding reaction to form $70S_I$ ribosomes (step 1), giving rise to a FRET signal with concomitant GTP hydrolysis (Figures 2B and 3A), is followed by a conformational change (step 2), resulting in formation of $70S_{II}$ ribosomes, from which P_i is released (step 3). In carrying out this fitting, we assume the light scattering increase due to $70S_I$, $70S_{II}$, or 70SIC formation is identical (*41*). Constraining the FRET efficiencies to also be the same for all three 70S species led to poor fits to the FRET data. However, setting the relative FRET efficiency (RFE) for 70SIC equal to 1.0 and allowing the RFEs of the other 70S species to be different led to best-fit values of 0.57 and 1.00 for $70S_I$ and $70S_{II}$, respectively. This point is made graphically in the inset of Figure 5A which shows that the ratio of normalized FRET change to normalized light scattering change increases as $70S_I$ is converted to $70S_{II}$ and does not change thereafter. We conclude that the L11-NTD moves closer to the G1 domain of IF2 as $70S_I$ is converted to $70S_{II}$, and that this movement follows GTP hydrolysis and precedes P_i release.

GTP Hydrolysis Accelerates the Increase in FRET Efficiency following 70S Formation. The previous conclusion led us to examine whether GTP hydrolysis was required for the increase in FRET efficiency within the 70S complex by replacing GTP with its nonhydrolyzable analogue GDPNP. We initially attempted to compare light scattering and FRET changes in the presence of GDPNP under conditions (50S > IF2 > 30S) exactly paralleling those we had used in the presence of GTP (Figure 5A). As seen in Figure 6A, replacement of GTP with GDPNP during 70SIC formation leads to only a small decrease in the magnitude of the light scattering increase, with little change in the rate of such an increase. However, these conditions are not suitable for measuring FRET changes during 70SIC formation, since a rapid and significant change in FRET signal is seen even in the absence of 70S formation [i.e., with fMet-$tRNA^{fMet}$ omitted (Figure 6B)], reflecting direct binding of Bst-$IF2^{Cy3}$·GDPNP to $50S^{Cy5}$. No such signal is seen in the presence of GTP (Figure 5A), because of the rapid hydrolysis of GTP within the 50S·IF2·GTP complex, and the relatively weak binding of IF2·GDP to 50S subunits (*20*).

Accordingly, FRET experiments were conducted under conditions (30S > IF2 > 50S) minimizing 50S·IF2·GDPNP formation, as seen by the very small FRET change when fMet-$tRNA^{fMet}$ is omitted (Figure 6C). Under these conditions, the total FRET change seen with GDPNP is similar to that seen with GTP, but the time development is different, with the initial increase occurring slightly faster with GDPNP and the full FRET change occurring much more slowly.

The light scattering results in the presence of GDPNP were well fit assuming biphasic kinetics. In contrast, fitting the FRET results required three phases and shows an approximate doubling in the apparent FRET efficiency during the slow third phase ($k_{app} \sim 0.2\ s^{-1}$) when, on the basis of the light scattering results, little additional 70S formation would be expected. Taken together, the results in panels A and C of Figure 6 are consistent with a kinetic scheme for 70SIC formation in the presence of GDPNP that is similar to Scheme 1 for GTP (Figure 5C), except that step 3 would be reversible and the increase in FRET efficiency following 70S formation occurs later in the process. It would thus appear that GTP hydrolysis accelerates, but is not essential for, the movement of the L11-NTD toward the G1 domain of IF2 as the initial 70S complex formed is converted to 70SIC.

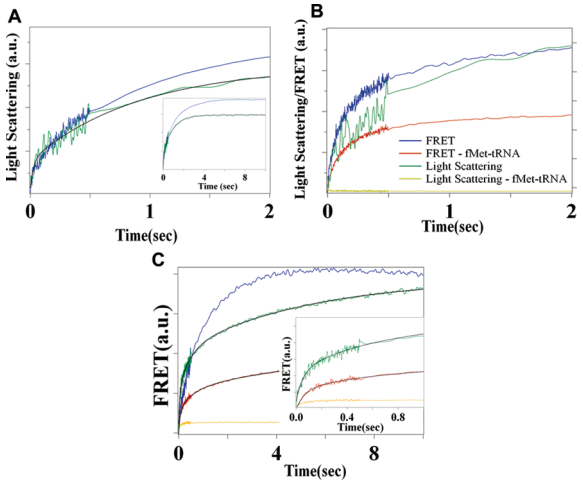

FIGURE 6: Measures of 70SIC formation when GDPNP replaces GTP. (A) Light scattering increase during 70SIC formation (blue trace, GTP; green trace, GDPNP). The inset shows extension of results to 10 s. (B) FRET efficiency and light scattering increases during 70SIC formation measured in the presence of GDPNP. FRET efficiencies are shown as blue and red traces in the presence and absence of fMet-$tRNA^{fMet}$, respectively. Light scattering is shown as green and yellow traces in the presence and absence of fMet-$tRNA^{fMet}$, respectively. (C) FRET efficiency increases during 70SIC formation. The blue trace is for the higher 30SIC concentration in the presence of GTP. Green and orange traces are for the higher 30SIC concentration in the presence of GDPNP in the presence and absence of fMet-$tRNA^{fMet}$, respectively. The red trace is for the lower 30SIC concentration in the presence of GDPNP. The inset shows an expanded time scale. Final concentrations in panels A and B were 0.3 μM 30S, 0.45 μM Bst-$IF2^{Cy3}$, and 0.60 μM $50S^{Cy5}$. Final concentrations in panel C were 0.6 μM 30S, 0.5 μM Bst-$IF2^{Cy3}$, and 0.18 μM $50S^{Cy5}$ (blue and green traces, higher 30SIC) or 0.3 μM 30S, 0.25 μM Bst-$IF2^{Cy3}$, and 0.18 μM $50S^{Cy5}$ (red trace, lower 30SIC). The final GTP or GDPNP concentration in panels A−C was 100 μM. Solid black lines are fits of the GDPNP results to either a two-phase (light scattering) or three-phase (FRET) reaction. Fitted parameter values are as follows: light scattering, k_{app1}, 35 ± 5 s^{-1}, k_{app2}, 1.10 ± 0.03 s^{-1}; FRET, higher 30SIC, k_{app1}, 20 ± 1 s^{-1}, k_{app2}, 2.2 ± 0.1 s^{-1}, k_{app3}, 0.19 ± 0.01 s^{-1}; relative FRET efficiency amplitudes, phase 1, 0.46 ± 0.05: phase 2, 0.51 ± 0.05: phase 3, 1.00; FRET, lower 30SIC, k_{app1}, 16 ± 1 s^{-1}, k_{app2}, 1.9 ± 0.1 s^{-1}, k_{app3}, 0.19 ± 0.01 s^{-1}; relative FRET efficiency amplitudes, phase 1, 0.64 ± 0.08: phase 2, 0.47 ± 0.06: phase 3, 1.00.

FRET Monitoring of the Fidelity Function of IF3. Earlier, we showed that the rate and magnitude of light scattering increase provided a sensitive measure of the ability of IF3 to discriminate between a canonical (AUG) and a noncanonical (AUU) initiation codon in 70SIC formation (*27*). The increase in FRET efficiency accompanying 70SIC formation also provides a sensitive probe of such discrimination (Figure 7). Thus, in the presence of IF3, substituting AUU (trace 3) for AUG (trace 1) leads to large decreases in both the rate and extent of FRET efficiency increase, whereas in the absence of IF3, the apparent rate is little affected and the extent of the increase is somewhat increased (traces 2 and 4). Identical trends were observed for light scattering changes (*27*).

DISCUSSION

IF2 is a G-protein that is part of 30SIC and is retained within the 70SIC that is formed following reaction of 30SIC with the 50S subunit (*11*, *12*). Here we show that FRET measurement of the interaction of IF2 with the L11-NTD can be used to monitor the relative motions of IF2 and the GTPase activation center during the process of 70SIC formation. We measure a FRET efficiency

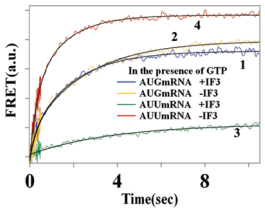

FIGURE 7: FRET monitoring of the fidelity function of IF3. The effect of IF3 on the rate and extent of FRET efficiency increase when the AUG initiation codon is replaced with AUU. 022AUG-mRNA, +IF3, blue trace; 022AUG-mRNA, −IF3, orange trace; 022AUU-mRNA, +IF3, green trace; 022AUU-mRNA, −IF3, red trace. Final concentrations were 0.15 μM IF2^{Cy3}, 0.3 μM 30S, 0.14 μM 50S^{Cy5}, and 100 μM GTP.

of 50% for the 70SIC complex, corresponding to an approximate fluorophore−fluorophore distance of 60 Å, equal to R_o (see Materials and Methods). This value is in reasonable accord with the distances of 50−55 Å between the α-carbons of residue 378 in Bst-IF2 and residue 38 in L11 that can be estimated from cryo-EM structures of 70S complexes containing fMet-tRNA^{fMet}, mRNA, and either IF2·GDPCP (another nonhydrolyzable analogue of GTP) or IF2·GDP (*11*), since the distances between the dyes would be expected to be somewhat greater than the distances between the α-carbons to which they are attached.

Although IF2·GDP binds to 70S ribosomes less tightly than IF2·GTP (*20*), consistent with the cryo-EM results of Myasnikov et al. (*11*) that indicate substantial differences in the overall interaction of IF2 with the 70S ribosome following GTP hydrolysis and P_i release, the results presented in Figure 5 indicate that the G1 domain of IF2 moves closer to L11-NTD as part of the process by which the complex initially formed from association of 50S with 30SIC, 70S$_I$·GDP·P_i in Scheme 1 (Figure 5C), is converted into the 70S$_{II}$·GDP·P_i complex, preceding P_i release and 70SIC formation. On the basis of the relative FRET efficiencies of 70S$_I$·GDP·P_i and 70S$_{II}$·GDP·P_i, we estimate this distance reduction to be ~12 Å (eq 3), i.e., from 72 to 60 Å.

$$R = R_o\left(\frac{1}{E} - 1\right)^{1/6} \quad (3)$$

Scheme 1 is a minimal kinetic scheme that accounts quantitatively for the results presented in Figure 5. It is fully consistent with the more complete scheme for 70SIC formation that we proposed previously (*20*, *27*), with the one minor change that the binding of 30SIC^{Cy3} to 50S^{Cy5} is 2−3-fold weaker than the binding to wt-50S. This earlier work, which employed a coumarin derivative of Bst-IF2, labeled at position 451, and fMet-tRNA^{fMet}(prf) (Figure 2D), demonstrated that conversion of the initially formed 70S complex to 70SIC required two conformational changes, corresponding approximately to steps 2 and 3 in Scheme 1, with step 2 involving a change in IF2 fluorescence and step 3 involving a change in fMet-tRNA^{fMet} fluorescence, the latter occurring at a rate very close to that of P_i release.

Results presented in Figure 7 show that FRET changes can be used to demonstrate the ability of IF3 to discriminate between a canonical (AUG) and a noncanonical (AUU) initiation codon in 70SIC formation and are consistent with the notion, proposed by us previously (*27*), that such discrimination occurs during 70SIC formation. This notion has recently received direct support from some rate measurements by Milon et al. (*43*) showing that 70S formation from 30SIC precedes IF3 dissociation and contrasts with results of Antoun et al. (*42*) indicating that dissociation of IF3 from 30SIC precedes 70S formation. It is likely that the reason for this apparent disagreement has to do with the strong dependence of the rates of these two processes on mRNA sequence. Thus, both our previous (*27*) and current studies and those of Milon et al. (*43*) employed ribosomes programmed with 022mRNA, which has a relatively short Shine−Dalgarno sequence (four nucleotides) separated from the AUG initiation codon by a long spacer (nine nucleotides) and affords relatively rapid 70SIC formation. However, Milon et al. also found that use of 002mRNA, which has a long Shine−Dalgarno sequence (nine nucleotides) and a shorter spacer (five nucleotides), leads to much slower 70S formation, which proceeds at the same rate as IF3 dissociation, consistent with the results of Antoun et al. (*42*), who used an mRNA similar to 002mRNA.

The 70S ribosome is a labile structure that undergoes conformational changes on the binding of the G-proteins EF-G and IF2. Cryoelectron microscopy studies (*11*, *12*) have shown not only that G-proteins bind to the same site on the 70S ribosome via their G(GTPase) domains but also that the conformational changes that result from G-protein binding as a GTP complex and from hydrolysis of the ribosome-bound GTP to GDP are similar for such proteins. This has led to the suggestion that ribosomal GTPases take advantage of the intrinsic flexibility of the ribosome to induce conformational changes that promote movement of mRNA and tRNA across the ribosome surface during the various steps of the protein synthesis cycle (*11*, *44*, *45*).

Our current and previous related studies provide strong evidence that the analogy between the structures of the complexes that at least two G-proteins, IF2 and EF-G, make with the ribosome is maintained on a dynamic level as well. In particular, the kinetics of FRET efficiency increase between fluorescent derivatives of the L11-NTD and either IF2 (labeled in the G1 domain, this work) or EF-G [labeled in the G′ domain (*15*)] have two important points in common. (1) The FRET efficiency increases, indicating a movement of the G-proteins toward the L11-NTD, following GTP hydrolysis and prior to P_i release (Figure 5), and (2) the rate of attainment of the higher-FRET efficiency state is considerably decreased upon substitution of a nonhydrolyzable analogue for GTP, although the total increase in FRET efficiency is maintained (Figure 6C). These two points provide strong evidence that at least some of the conformational changes attributed to GTPase activity are triggered by the hydrolysis step itself, rather than by P_i release, in accord with earlier suggestions (*36*, *46*, *47*), and that the high FRET efficiency state is the preferred mode of binding of G-protein to the 70S ribosome.

REFERENCES

1. Gualerzi, C. O., and Pon, C. L. (1990) Initiation of mRNA translation in prokaryotes. *Biochemistry 29*, 5881–5889.
2. Boelens, R., and Gualerzi, C. O. (2002) Structure and function of bacterial initiation factors. *Curr. Protein Pept. Sci. 3*, 107–119.
3. Ramakrishnan, V. A. (2002) Ribosome structure and the mechanism of translation. *Cell 108*, 557–572.
4. Laursen, B. S., Sorensen, H. P., Mortensen, K. K., and Sperling-Petersen, H. U. (2005) Initiation of protein synthesis in bacteria. *Microbiol. Mol. Biol. Rev. 69*, 101–123.
5. Gualerzi, C. O., Brandi, L., Caserta, E., Garofalo, C., Lammi, M., La Teana, A., Petrelli, D., Spurio, R., Tomsic, J., and Pon, C. L. (2001) Role of the initiation factors in the early events of mRNA translation in bacteria. *Cold Spring Harbor Symp. Quant. Biol. 66*, 363–376.
6. Li, W., Sengupta, J., Rath, B. K., and Frank, J. (2006) Functional conformations of the L11-ribosomal RNA complex revealed by correlative analysis of cryo-EM and molecular dynamics simulations. *RNA 12*, 1240–1253.

7. Connell, S. R., Takemoto, C., Wilson, D. N., Wang, H., Murayama, K., Terada, T., Shirouzu, M., Rost, M., Schüler, M., and Giesebrecht, J.; et al. (2007) Structural basis for interaction of the ribosome with the switch regions of GTP-bound elongation factors. *Mol. Cell 25*, 751–764.
8. Agrawal, R. K., Heagle, A. B., Penczek, P., Grassucci, R. A., and Frank, J. (1999) EF-G-dependent GTP hydrolysis induces translocation accompanied by large conformational changes in the 70S ribosome. *Nat. Struct. Biol. 6*, 643–647.
9. Agrawal, R. K., Linde, J., Sengupta, J., Nierhaus, K. H., and Frank, J. (2001) Localization of L11 protein on the ribosome and elucidation of its involvement in EF-G-dependent translocation. *J. Mol. Biol. 311*, 777–787.
10. Frank, J., and Agrawal, R. K. (2000) A ratchet-like inter-subunit reorganization of the ribosome during translocation. *Nature 406*, 318–322.
11. Myasnikov, A. G., Marzi, S., Simonetti, A., Giuliodori, A. M., Gualerzi, C. O., Yusupova, G., Yusupov, M., and Klaholz, B. P. (2005) Conformational transition of initiation factor 2 from the GTP- to GDP-bound state visualized on the ribosome. *Nat. Struct. Mol. Biol. 12*, 1145–1149.
12. Allen, G. S., Zavialov, A., Gursky, R., Ehrenberg, M., and Frank, J. (2005) The cryo-EM structure of a translation initiation complex from *Escherichia coli*. *Cell 121*, 703–712.
13. Diaconu, M., Kothe, U., Schlünzen, F., Fischer, N., Harms, J. M., Tonevitsky, A. G., Stark, H., Rodnina, M. V., and Wahl, M. C. (2005) Structural basis for the function of the ribosomal L7/12 stalk in factor binding and GTPase activation. *Cell 121*, 991–1004.
14. Schuwirth, B. S., Borovinskaya, M. A., Hau, C. W., Zhang, W., Vila-Sanjurjo, A., Holton, J. M., and Cate, J. H. (2005) Structures of the bacterial ribosome at 3.5 Å resolution. *Science 310*, 827–834.
15. Seo, H., Abedin, S., Kamp, D., Wilson, D. N., Nierhaus, K. H., and Cooperman, B. S. (2006) EF-G-Dependent GTPase on the ribosome. Conformational change and fusidic acid inhibition. *Biochemistry 45*, 2504–2514.
16. Marzi, S., Knight, W., Brandi, L., Caserta, E., Soboleva, N., Hill, W. E., Gualerzi, C. O., and Lodmell, J. S. (2003) Ribosomal localization of translation initiation factor IF2. *RNA 9*, 958–969.
17. La Teana, A., Pon, C. L., and Gualerzi, C. O. (1996) Late events in translation initiation. Adjustment of fMet-tRNA in the ribosomal P-site. *J. Mol. Biol. 256*, 667–675.
18. Wu, X. Q., and RajBhandary, U. L. (1997) Effect of the amino acid attached to *Escherichia coli* initiator tRNA on its affinity for the initiation factor IF2 and on the IF2 dependence of its binding to the ribosome. *J. Biol. Chem. 272*, 1891–1895.
19. Brombach, M., Gualerzi, C. O., Nakamura, Y., and Pon, C. L. (1986) Molecular cloning and sequence of the *Bacillus stearothermophilus* translational initiation factor IF2 gene. *Mol. Gen. Genet. 205*, 97–102.
20. Grigoriadou, C., Marzi, S., Kirillov, S., Gualerzi, C. O., and Cooperman, B. S. (2007) A quantitative kinetic scheme for 70 S translation initiation complex formation. *J. Mol. Biol. 373*, 562–572.
21. La Teana, A., Pon, C. L., and Gualerzi, C. O. (1993) Translation of mRNAs with degenerate initiation triplet AUU displays high initiation factor 2 dependence and is subject to initiation factor 3 repression. *Proc. Natl. Acad. Sci. U.S.A. 90*, 4161–4165.
22. Spurio, R., Brandi, L., Caserta, E., Pon, C. L., Gualerzi C. O., Misselwitz, R., Kraffti, C., Welflei, K., and Welflei, H. (2000) The C-terminal subdomain (IF2 C-2) contains the entire fMet-tRNA binding site of initiation factor IF2. *J. Biol. Chem. 275*, 2447–2454.
23. Pan, D., Kirillov, S., Zhang, C. M., Hou, Y. M., and Cooperman, B. S. (2006) Rapid ribosomal translocation depends on the conserved 18−55 base pair in P-site transfer RNA. *Nat. Struct. Mol. Biol. 13*, 354–359.
24. Mujumdar, R. B., Ernst, L. A., Mujumdar, S. R., Lewis, C. J., and Waggoner, A. S. (1993) Cyanine Dye Labeling Reagents: Sulfoindocyanine Succinimidyl Esters. *Bioconjugate Chem. 4*, 105–111.
25. Bradford, M. M. (1976) A rapid and sensitive method for the quantitation of microgram quantities of protein utilizing the principle of protein-dye binding. *Anal. Biochem. 72*, 248–254.
26. Wang, Y., Qin, H., Kudaravalli, R. D., Kirillov, S. V., Dempsey, G. T., Pan, D., Cooperman, B. S., and Goldman, Y. E. (2007) Single-molecule structural dynamics of EF-G-ribosome interaction during translocation. *Biochemistry 46*, 10767–10775.
27. Grigoriadou, C., Marzi, S., Pan, D., Gualerzi, C. O., and Cooperman, B. S. (2007) The translational fdelity function of IF3 during transition from the 30 S initiation complex to the 70 S initiation complex. *J. Mol. Biol. 373*, 551–561.
28. Rodnina, M. V., Semenkov, Y. P., and Wintermeyer, W. (1994) Purification of fMet-tRNA(fMet) by fast protein liquid chromatography. *Anal. Biochem. 219*, 380–381.
29. Pan, D., Kirillov, S. V., and Cooperman, B. S. (2007) Kinetically competent intermediates in the translocation step of protein synthesis. *Mol. Cell 25*, 519–529.
30. Harris, D. C. (1995) *Quantitative Chemical Analysis*, 4th ed., W. H. Freeman and Company, New York. .
31. Lakowicz, J. R. (1999) *Principles of Fluorescence Spectroscopy*, 2nd ed., Kluwer Academic/Plenum Press, New York. .
32. dos Remedios, C. G., and Moens, P. D. (1995) Fluorescence resonance energy transfer spectroscopy is a reliable "ruler" for measuring structural changes in proteins. Dispelling the problem of the unknown orientation factor. *J. Struct. Biol. 115*, 175–185.
33. Blanchard, S. C., Kim, H. D., Gonzalez, R. L.Jr., Puglisi, J. D., and Chu, S. (2004) tRNA dynamics on the ribosome during translation. *Proc. Natl. Acad. Sci. U.S.A. 101*, 12893–12898.
34. Yasuda, R., Masaike, T., Adachi, K., Noji, H., Itoh, H., and Kinosita, K.Jr. (2003) The ATP-waiting conformation of rotating F1-ATPase revealed by single-pair fluorescence resonance energy transfer. *Proc. Natl. Acad. Sci. U.S.A. 100*, 9314–9318.
35. Qin, H., Marzi, S., and Cooperman, B. S. (2008) Simultaneous binding of G-proteins to the ribosome, manuscript in preparation.
36. Tomsic, J., Vitali, L. A., Daviter, T., Savelsbergh, A., Spurio, R., Striebeck, P., Wintermeyer, W., Rodnina, M. V., and Gualerzi, C. O. (2000) Late events of translation initiation in bacteria: A kinetic analysis. *EMBO J. 19*, 2127–2136.
37. Naaktgeboren, N., Schrier, P., Möller, W., and Voorma, H. O. (1976) The involvement of protein L11 in the joining of the 30-S initiation complex to the 50-S subunit. *Eur. J. Biochem. 62*, 117–123.
38. Götz, F., Fleischer, C., Pon, C. L., and Gualerzi, C. O. (1989) Subunit association defects in *Escherichia coli* ribosome mutants lacking proteins S20 and L11. *Eur. J. Biochem. 183*, 19–24.
39. Cundliffe, E., Dixon, P., Stark, M., Stöffler, G., Ehrlich, R., Stöffler-Meilicke, M., and Cannon, M. (1979) Ribosomes in thiostrepton-resistant mutants of *Bacillus megaterium* lacking a single 50 S subunit protein. *J. Mol. Biol. 132*, 235–252.
40. Cohlberg, J. A., and Nomura, M. (1976) Reconstitution of *Bacillus stearothermophilus* 50 S ribosomal subunits from purified molecular components. *J. Biol. Chem. 251*, 209–221.
41. Antoun, A., Pavlov, M. Y., Andersson, K., Tenson, T., and Ehrenberg, M. (2004) Ribosome formation from subunits studied by stopped-flow and Rayleigh light-scattering. *Biol. Proced. Online 6*, 35–54.
42. Antoun, A., Pavlov, M. Y., Lovmar, M., and Ehrenberg, M. (2006) How initiation factors tune the rate of initiation of protein synthesis in bacteria. *EMBO J. 25*, 2539–2550.
43. Milon, P., Konevega, A. L., Gualerzi, C. O., and Rodnina, M. V. (2008) Kinetic checkpoint at a late step in translation initiation. *Mol. Cell 30*, 712–720.
44. Frank, J., Gao, H., Sengupta, J., Gao, N., and Taylor, D. J. (2007) The process of mRNA-tRNA translocation. *Proc. Natl. Acad. Sci. U. S.A. 104*, 19671–19678.
45. Cornish, P. V., Ermolenko, D. N., Noller, H. F., and Ha, T. (2008) Spontaneous intersubunit rotation in single ribosomes. *Mol. Cell 30*, 578–588.
46. Rodnina, M. V., Savelsbergh, A., Katunin, V. I., and Wintermeyer, W. (1997) Hydrolysis of GTP by elongation factor G drives tRNA movement on the ribosome. *Nature 385*, 37–41.
47. Savelsbergh, A., Katunin, V. I., Mohr, D., Peske, F., Rodnina, M. V., and Wintermeyer, W. (2003) An elongation factor G-induced ribosome rearrangement precedes tRNA-mRNA translocation. *Mol. Cell 11*, 1517–1523.